The Shape of the Ribosome Exit Tunnel Affects Cotranslational Protein Folding

Renuka Kudva[1], Fátima Pardo-Avila[2], Hena Sandhu[1], Marta Carroni[1,3], Harris D. Bernstein[4], Gunnar von Heijne[1,3*]

[1]Department of Biochemistry and Biophysics, Stockholm University, SE-106 91 Stockholm, Sweden

[2]Department of Structural Biology, Stanford University, Stanford, CA 94085, USA

[3] Science for Life Laboratory Stockholm University, Box 1031, SE-171 21 Solna, Sweden

[4]Genetics and Biochemistry Branch, National Institute of Diabetes and Digestive and Kidney Diseases, National Institutes of Health, Bethesda, MD 20892, USA

*To whom correspondence should be addressed:

Phone: Int+46-8-16 25 90. E-mail: gunnar@dbb.su.se

Classification: Biological sciences; Biochemistry

Key words: protein folding, ribosome, cotranslational, arrest peptide, uL23, uL24

Running title: Cotranslational protein folding

Abbreviations: AP = arrest peptide

Abstract

The *Escherichia coli* ribosome exit tunnel can accommodate small folded proteins, while larger ones tend to fold outside. It remains unclear, however, to what extent the geometry of the tunnel influences protein folding. Here, using ribosomes with deletions in proteins uL23 and uL24, we investigate how tunnel geometry determines where proteins of different sizes fold. We find that a 29-residue zinc-finger domain folding close to the uL23 loop in wildtype ribosomes folds deeper in the tunnel in uL23 Δloop (but not in uL24 Δloop) ribosomes, while two ~100-residue domains that fold close to the uL24 loop near the tunnel exit in wildtype ribosomes fold at deeper locations in uL24 Δloop (but not in uL23 Δloop) ribosomes. These results provide strong support to the idea that cotranslational folding commences once a protein domain reaches a location in the exit tunnel where there is sufficient space to house the folded structure.

Introduction

A large fraction of cellular proteins likely start to fold cotranslationally in the ~100 Å long exit tunnel in the ribosomal large subunit (1-3), before they emerge into the cytosolic environment. In bacterial ribosomes, portions of the 23S rRNA and a few universally conserved proteins line the exit tunnel, Fig. 1a. The tunnel proteins uL4, uL22, and uL23 consist of globular domains that are buried within the rRNA, and β-hairpin loops that protrude into the tunnel (4). These loops help stabilize the tertiary structure of 23S rRNA (5) and contribute towards the unique geometry of the tunnel (2, 6, 7). uL24 and uL29 are located near the end of the tunnel, and a hairpin loop in uL24 partially obstructs the tunnel exit.

Inspired by our observations that the small ADR1a domain folds deep within the exit tunnel (8-10) while the larger titin and spectrin domains fold in the mouth of the tunnel (11, 12), we now ask what role the geometry of the exit tunnel plays in determining where these domains fold. To explore this question, we employ the same arrest peptide-based approach used in our previous studies of cotranslational protein folding (8, 11), but with ribosomes that carry deletions in either the uL23 or the uL24 loop. Our findings provide strong evidence that the tunnel geometry determines where in the tunnel a protein starts to fold.

Results and Discussion

The folding assay

Our experimental set-up, Fig. 1b, exploits the ability of the SecM translational arrest peptide (AP) (13) to act as a force sensor (14-16), making it possible to detect the folding of protein domains in the exit tunnel (8, 16). In brief, the domain to be studied is cloned, via a linker, to the AP, *L* residues away from its

63 terminal proline. The AP is followed by a C-terminal tail, to ensure that arrested
64 (*A*) nascent chains can be separated from full-length (*FL*) chains by SDS-PAGE.
65 Constructs with different *L* are translated in the PURE *in vitro* translation system
66 (17), and the fraction full-length protein (f_{FL}) is determined for each *L*. For
67 linkers that, when stretched, are long enough to allow the protein to reach a part
68 of the exit tunnel where it can fold, force will be exerted on the AP by the folding
69 protein, reducing stalling and increasing f_{FL}. (12), Fig. 1c. A plot of f_{FL} vs. *L* thus
70 shows where in the exit tunnel a protein starts to fold and at which linker length
71 folding no longer causes increased tension in the nascent chain.

72 *uL23 Δloop and uL24 Δloop ribosomes*

73 The *E. coli* strains HDB143 (uL23 Δloop; uL23 residues 65-74 deleted) and
74 HDB144 (uL24 Δloop; uL24 residues 43-57 deleted) are viable (18), as is a strain
75 where uL23 has been replaced by a homologue from spinach chloroplast
76 ribosomes that also lacks the β-hairpin loop (19, 20). The HDB140 (wt), HDB143
77 and HDB144 strains were used to purify high-salt-washed ribosomes that were
78 used to translate proteins in the commercially available PURExpress® Δ-
79 Ribosome kit. Analysis of the purified ribosomes by SDS-PAGE and Western
80 blotting demonstrated the expected size differences compared to wildtype for
81 the uL23 Δloop and uL24 Δloop proteins, Supplementary Fig. S1.

82 *Cryo-EM structure of uL23 Δloop ribosomes*

83 The loop deleted in the uL24 Δloop ribosomes does not interact with
84 neighboring parts of the ribosome, Fig. 2a, and hence its removal would not be
85 expected to alter the structure of other parts of the exit tunnel. In contrast, the
86 loop deleted in uL23 Δloop ribosomes is located deep in the exit tunnel, Fig. 2b,

87 and it is not clear *a priori* whether its removal may cause rearrangements in
88 other tunnel components. For this reason, we purified uL23 Δloop ribosomes
89 and determined a cryo-EM structure at an average resolution of 3.3 Å, Fig. 2c,
90 Supplementary Fig. S2. The only significant difference between the uL23 map
91 and previously reported *E. coli* ribosome maps is the absence of the deleted part
92 of uL23, Fig. 2d. The shape of the tunnel remains unchanged in the uL23 Δloop
93 ribosome, except for the increase in volume caused by the absence of the uL23
94 loop. To estimate the volume increase, we employed the POVME algorithm (21,
95 22). Compared to the wildtype *E. coli* ribosome, the tunnel volume is increased
96 by 2,064 $Å^3$ in the uL23 Δloop ribosome, about 1/3 of the size of ADR1a (5,880
97 $Å^3$) calculated by the same method, see Supplementary Movie.

98 *ADR1a folds deeper in the exit tunnel in uL23 Δloop but not in uL24 Δloop*
99 *ribosomes*

100 ADR1a constructs of different linker lengths were translated in the
101 PURExpress® Δ-Ribosome kit supplemented with purified wildtype, uL23 Δloop,
102 or uL24 Δloop ribosomes, either in the presence of 50 μM Zn^{2+} (to promote
103 folding of ADR1a) or in the presence of 50 μM of the zinc-specific chelating agent
104 TPEN (to prevent folding of ADR1a). As a control, we also translated all
105 constructs in the PURExpress® kit including wildtype ribosomes provided by
106 the manufacturer.

107 Similar to previous results (8), we saw efficient stalling in the presence of TPEN
108 at $L \geq 19$ residues, Fig. 3a. In order to compensate for the increase in f_{FL} seen at L
109 = 17 residues in the presence of TPEN (hence not related to folding), we plotted
110 $\Delta f_{FL} = f_{FL}(Zn^{2+}) - f_{FL}(\text{TPEN})$, Fig. 3b. In the presence of Zn^{2+}, the Δf_{FL} profiles for

111 wildtype and uL24 Δloop ribosomes were identical within experimental error:
112 Δf_{FL} starts to increase around L = 20 residues and peaks at L = 25 residues (gray,
113 gray dashed, and blue curves). In contrast, for the uL23 Δloop ribosomes, Δf_{FL}
114 starts to increase already at L = 17 residues and peaks at L = 21-25 residues (red
115 curve).

116 A previous cryo-EM study demonstrated that ADR1a folds deep inside the
117 ribosome exit tunnel in a location where it is in contact with the uL23 loop (8),
118 Fig. 2b. The additional space available in uL23 Δloop ribosomes thus makes it
119 possible for ADR1a to fold at 2-3 residues shorter linker lengths. Assuming an
120 extended conformation of the linker segment (~3Å per residue), this means that
121 ADR1a folds ~6-9 Å deeper in the exit tunnel in uL23 Δloop ribosomes than in
122 wildtype ribosomes.

123 *Spectrin and titin domains fold deeper in the exit tunnel in uL24 Δloop ribosomes*

124 α-spectrin domains R15 and R16 have been shown to fold cotranslationally (11),
125 with R15 folding at L = 35-41 residues and R16 folding at L = 29-35 residues, in
126 close proximity to uL24 (11).

127 As seen in Fig. 3c, the f_{FL} profiles show that spectrin R15 starts to fold at L = 35
128 residues both in wildtype and uL23 Δloop ribosomes (gray and red curves,
129 respectively) and f_{FL} peaks at L = 41 residues, as has been observed previously
130 (11). The slight dip at L = 37 residues might reflect an early folding intermediate.
131 In uL24 Δloop ribosomes spectrin R15 also starts to fold at L = 35 residues, but
132 f_{FL} peaks already at L = 37 residues (blue curve).

133 For R16, f_{FL} starts to increase at L = 29 residues and peaks at L = 35 residues for
134 wildtype and uL23 Δloop ribosomes, Fig. 3d. For uL24 Δloop ribosomes however,

135 f_{FL} starts to rise earlier and peaks already at L = 31-33 residues, suggesting that
136 that spectrin R16 folds at 2-3 residues shorter linker lengths, ~6-9 Å deeper in
137 the exit tunnel.

138 Interestingly, while the shapes of the f_{FL} profiles for R15 obtained with wildtype
139 and uL23 Δloop ribosomes are nearly identical, the uL23 Δloop profile has an
140 approximately 1.5-fold lower amplitude. We speculate that the wider tunnel in
141 the uL23 Δloop ribosome allows more flexibility in the linker segment, lowering
142 its "spring constant" such that a given amount of stretching induces less tension
143 in the AP.

144 Similar results were obtained for the 89-residue titin I27 domain, Fig. 3e.
145 Previous studies have shown that the I27 domain folds at linker lengths L = 35-
146 39 residues and in about the same location as does spectrin R16, in close
147 proximity to the uL24 loop (12). The f_{FL} profile is not affected by the uL23 loop
148 deletion, but folding commences at 2-3 residues shorter linker lengths in uL24
149 Δloop ribosomes.

150 Our results are consistent with the idea that proteins start to fold as soon as they
151 reach a part of the exit tunnel that is wide enough to hold the folded protein.
152 Thus, the 29-residue ADR1a domain folds ~6-9 Å deeper in the exit tunnel in
153 uL23 Δloop ribosomes than in wildtype and uL24 Δloop ribosomes, while the 89-
154 and 109-residue titin and spectrin domains fold ~6-9 Å deeper inside the tunnel
155 in uL24 Δloop ribosomes than in wildtype and uL23 Δloop ribosomes.

156 Both the uL23 and uL24 loops thus serve to reduce the space available for
157 folding, but in different parts of the exit tunnel. The uL24 loop is particularly
158 interesting in this regard. It partially blocks the tunnel exit, closing off what

159 would otherwise be a wide, funnel-like opening, Fig. 2a, and may prevent
160 premature folding of domains that would otherwise misfold in the tunnel, or that
161 depend on interactions with trigger factor (23, 24) for efficient folding. It has
162 recently been shown to interact with the titin I27 domain during cotranslational
163 folding (12). The uL24 loop is conserved (in length, if not in sequence) in
164 bacterial ribosomes, suggesting that it affects cotranslational protein folding not
165 only in *E. coli*, but in bacteria in general.

166

167 **Acknowledgements**

168 This work was supported by grants from the Knut and Alice Wallenberg
169 Foundation, the Swedish Cancer Foundation, and the Swedish Research Council
170 to GvH, and the Intramural Research program of the National Institute of
171 Diabetes and Digestive and Kidney Diseases to HDB. FPA was supported by NIH
172 grant R35GM122543. The cryo-EM data were collected at the Swedish National
173 Cryo-EM Facility funded by the Knut and Alice Wallenberg Foundation, the
174 Family Erling Persson Foundation and the Science for Life Laboratory.

175

176 **Materials and Methods**

177 *Enzymes and Chemicals*

178 The PURExpress® Δ Ribosome and the PURExpress® kits were purchased from
179 New England Biolabs (Cat no. E3313S and E6800S respectively). The
180 components used to prepare Lysogeny Broth (LB Medium) for ribosome
181 isolation were obtained from BD Biosciences, cOmplete™ protease inhibitor from

182 Roche, and all other chemicals used were sourced from Merck Sigma Aldrich.
183 (^{35}S) Methionine was purchased from Perkin Elmer. Bis-Tris gels and plasmid
184 isolation kits were obtained from Thermo Scientific.

185 *Plasmids*

186 All ADR1, spectrin and titin constructs fused to the *E. coli* SecM AP via a variable
187 linker were expressed from the pET19b vector, as described previously (8, 11,
188 12). The spectrin constructs used in this study lacked the soluble domain of LepB
189 at the N-terminus.

190 *Strains and antisera*

191 Strains HDB140 (referred to as wildtype), HDB143 (referred to as uL23 Δloop)
192 and HDB144 (referred to as uL24 Δloop), as well as rabbit polyclonal antisera
193 against uL23 and uL24, are described in (18).

194 *Isolation of ribosomes*

195 Ribosomes were purified from the strains HDB140, HDB143, and HDB144. The
196 strains were cultured in Lysogeny broth (LB) to an A_{600} of 1.0 at 37°C and chilled
197 on ice for 15 min before they were harvested by centrifugation at 4000 g for 10
198 min. The cell pellet was washed twice with Buffer A at pH 7.5 (10 mM Tris-OAc,
199 14 mM $Mg(OAc)_2$, 60 mM KOAc, 1 mM DTT, 0.1% cOmplete™ Protease Inhibitor)
200 and lysed using the Emulsifex (Avestin) at a pressure of 8000 psi. The cell lysate
201 was loaded on a sucrose cushion at pH 7.5 (50 mM Tris-OAc, 1 M KOAc, 15 mM
202 $Mg(OAc)_2$, 1.44 M Sucrose, 1 mM DTT, 0.1% cOmplete™ Protease Inhibitor) and
203 centrifuged at 80,000xg in a Ti70 rotor (Beckman-Coulter) for 17 hours. The
204 obtained ribosomal pellet was resuspended in Buffer B at pH 7.5 (50 mM Tris-

205 OAc, 50 mM KOAc, 5 mM $Mg(OAc)_2$, 1 mM DTT), flask frozen in liquid nitrogen
206 and stored at -80°C.

207 Each batch of ribosomes that was prepared was tested for optimal translation by
208 titrating different volumes in the PURExpress ® Δ-Ribosome kit.

209 *In vitro transcription and translation*

210 The generated constructs were translated for 20 min. in the PURExpress® Δ-
211 Ribosome kit supplemented with high-salt-washed ribosomes isolated from
212 HDB140, HDB143 (uL23 Δloop), or HDB144 (uL24 Δloop). ADR1-SecM
213 constructs were also labelled in the PURExpress® kit to compare translation
214 with our purified wildtype ribosomes.

215 Plasmid DNA of each construct (300 ng) was used as a template for polypeptide
216 synthesis, and translation was carried out in the presence of (^{35}S) Methionine at
217 37°C for 20 min at 500 r.p.m. For ADR1a constructs, the translation reactions
218 also included either 50 μM $ZnCl_2$ or 50 μM of the Zn^{2+} chelator TPEN. Translation
219 was stopped by treating the sample with a final concentration of 5%
220 trichloroacetic acid (TCA) and incubated on ice for 30 min. The TCA precipitated
221 samples were subsequently centrifuged at 20,000 g for 10 min in a tabletop
222 centrifuge (Eppendorf) and the pellet obtained was solubilized in sample buffer,
223 supplemented with RNaseA (400 μg/ml), and incubated at 37°C for 15 minutes.
224 The samples were resolved on 12% Bis-Tris gels (Thermo Scientific) in MOPS
225 buffer for ADR1 and MES buffer for Spectrin and Titin. Gels were dried and
226 subjected to autoradiography and scanned using the Fujifilm FLA-9000
227 phosphorimager for visualization of radioactively labeled translated proteins.

228 *Quantification of radioactively labelled proteins*

229 The protein bands on the gel were quantified using MultiGauge (Fujifilm) from
230 which one-dimensional intensity profiles of each gel lane was extracted. This
231 information was subsequently fit to a Gaussian distribution using EasyQuant
232 (Rickard Hedman, Stockholm University). The sum of the arrested and full-length
233 bands was calculated, and this was used to estimate the fraction full-length
234 protein for each construct.

235 *Cryo-EM sample preparation and data processing*

236 The uL23 Δloop ribosomes (4 A_{260}/ml) were loaded on Pelco® TEM 400 mesh
237 Cu grids pre-coated with 2 nm thick carbon and frozen using the Vitrobot Mark
238 IV (FEI). Data was collected on the Titan Krios (FEI) microscope operated at 300
239 keV and equipped with a Falcon II direct electron detector. The camera was set
240 to a nominal magnification of 75,000X, which resulted in a pixel size of 1.09 Å at
241 the sample level and a defocus range of -1 to -3 μm.

242 The frame dose used was 1.17 e/$Å^2$, and 20 frames were aligned using
243 MotionCor2 (25) within the Scipion software suite (26). The micrographs were
244 visually inspected and those within a resolution threshold of 5 Å were selected,
245 yielding 3522 micrographs.

246 471272 particles were picked using Xmipp manual-pick followed by particle
247 extraction within Scipion and further processing in CryoSPARC (27). Two rounds
248 of 2D classification were done and 297,363 particles were subjected to *ab initio*
249 reconstruction into 3 classes to further sort out heterogeneity. A single
250 homogeneous class consisting of 132,029 particles was used for final
251 homogeneous refinement that resulted in a final map with an average FSC

252 resolution at 0.143 of 3.28 Å. The obtained map was sharpened and corrected for
253 handedness in CryoSPARC fitted with PDBs 3JBU and 4YBB in Chimera (28).
254 Local resolution and FSC at 0.143 was estimated in cryoSPARC. The electron
255 microscopy map was deposited in the Electron Microscopy Data Bank and
256 assigned the ID EMD-4319.

257 The initial model for uL23 Δloop was built with Coot, and improved by energy
258 minimization in a solvated dodecahedron box of explicit TIP3P waters,
259 neutralized with chloride ions and using the Amber 99SB-ILDN force field (29).
260 The steepest descent minimization method implemented in GROMACS 2016.1
261 was used (30, 31). Even after minimization, the backbone of the new loop formed
262 after the deletion of residues 65-74 still showed improper geometry and
263 Ramachandran outliers, and kinematic sampling (32) was performed to model
264 alternative loop conformations, and the loop that could fit the electron density
265 and had the best Ramachandran score was selected. The final model was
266 deposited as PDB 6FU8.

267 Figures were prepared using MacPymol 1.8.6.2 (Schrödinger LLC), Chimera (28),
268 and ChimeraX (33).

269 *Calculation of tunnel volume*

270 The volume calculations were performed with POVME 2.0 (1), using the *E. coli*
271 SecM structure PDB 3JBU as a reference. A series of overlapping spheres- eight
272 with a 20 Å radius, and one with a 40 Å radius were generated to determine the
273 inclusion region of the tunnel. In order to have a complete coverage of the exit
274 tunnel, the centers of the spheres were chosen to match the coordinates
275 corresponding to alternating Cα atoms of the amino acids of the SecM arrest

276 peptide located within the exit tunnel (for the 20 Å radius spheres the residues
277 use as centers were D11, F13, T15, V17, I19, Q21, Q23, I25, A27, G28 and for the
278 40 Å radius sphere the residue was E3). Grid Spacing was set to 2.0 Å, and the
279 distance cut-off to 1.09 Å. For all three cases (wildtype, uL24 Δ loop, uL23 Δ
280 loop), the region of inclusion used was the same, and the SecM arrest peptide
281 located within the exit tunnel was removed. For uL23 Δloop ribosomes residues
282 65-74 were removed from uL23, and for uL24 Δloop ribosomes residues 43-57
283 were removed from uL24 (numbering based on PDB 3JBU) prior to the
284 calculation.

285

286 **References**

287 1. Milligan RA & Unwin PN (1986) Location of exit channel for nascent
288 protein in 80S ribosome. *Nature* 319:693-695.
289 2. Ban N, Nissen P, Hansen J, Moore PB, & Steitz TA (2000) The complete
290 atomic structure of the large ribosomal subunit at 2.4 A resolution.
291 *Science* 289:905-920.
292 3. Nissen P, Hansen J, Ban N, Moore PB, & Steitz TA (2000) The structural
293 basis of ribosome activity in peptide bond synthesis. *Science* 289:920-930.
294 4. Klein DJ, Moore PB, & Steitz TA (2004) The roles of ribosomal proteins in
295 the structure assembly, and evolution of the large ribosomal subunit. *J*
296 *Mol Biol* 340:141-177.
297 5. Lawrence MG*, et al.* (2016) The extended loops of ribosomal proteins uL4
298 and uL22 of Escherichia coli contribute to ribosome assembly and protein
299 translation. *Nucleic Acids Res* 44:5798-5810.

300 6. Nissen P, Hansen J, Ban N, Moore P, & Steitz T (2000) The structural basis
301 of ribosome activity in protein synthesis. *Science* 289:920-930.
302 7. Harms J, *et al.* (2001) High resolution structure of the large ribosomal
303 subunit from a mesophilic eubacterium. *Cell* 107:679-688.
304 8. Nilsson OB, *et al.* (2015) Cotranslational protein folding inside the
305 ribosome exit tunnel. *Cell reports* 12:1533-1540.
306 9. Farias-Rico JA, Goetz SK, Marino J, & von Heijne G (2017) Mutational
307 analysis of protein folding inside the ribosome exit tunnel. *FEBS Lett*
308 591:155-163.
309 10. Nilsson OB, Müller-Lucks A, Kramer G, Bukau B, & von Heijne G (2016)
310 Trigger factor reduces the force exerted on the nascent chain by a
311 cotranslationally folding protein. *J Mol Biol* 428:1356-1364.
312 11. Nilsson OB, *et al.* (2017) Cotranslational folding of spectrin domains via
313 partially structured states. *Nat Struct Mol Biol* 24:221-225.
314 12. Tian P, *et al.* (2018) The folding pathway of an Ig domain is conserved on
315 and off the ribosome. *BioRxiv* doi: https://doi.org/10.1101/253013.
316 13. Nakatogawa H & Ito K (2001) Secretion monitor, SecM, undergoes self-
317 translation arrest in the cytosol. *Mol Cell* 7:185-192.
318 14. Ismail N, Hedman R, Lindén M, & von Heijne G (2015) Charge-driven
319 dynamics of nascent-chain movement through the SecYEG translocon. *Nat*
320 *Struct Mol Biol* 22:145-149.
321 15. Ismail N, Hedman R, Schiller N, & von Heijne G (2012) A biphasic pulling
322 force acts on transmembrane helices during translocon-mediated
323 membrane integration. *Nature Struct Molec Biol* 19:1018-1022.

324 16. Goldman DH, *et al.* (2015) Mechanical force releases nascent chain-
325 mediated ribosome arrest *in vitro* and *in vivo*. *Science* 348:457-460.
326 17. Shimizu Y, Kanamori T, & Ueda T (2005) Protein synthesis by pure
327 translation systems. *Methods* 36:299-304.
328 18. Peterson JH, Woolhead CA, & Bernstein HD (2010) The conformation of a
329 nascent polypeptide inside the ribosome tunnel affects protein targeting
330 and protein folding. *Mol Microbiol* 78:203-217.
331 19. Bubunenko MG, Schmidt J, & Subramanian AR (1994) Protein substitution
332 in chloroplast ribosome evolution. A eukaryotic cytosolic protein has
333 replaced its organelle homologue (L23) in spinach. *J Mol Biol* 240:28-41.
334 20. Bieri P, Leibundgut M, Saurer M, Boehringer D, & Ban N (2017) The
335 complete structure of the chloroplast 70S ribosome in complex with
336 translation factor pY. *EMBO J* 36:475-486.
337 21. Durrant JD, de Oliveira CA, & McCammon JA (2011) POVME: an algorithm
338 for measuring binding-pocket volumes. *J Mol Graph Model* 29:773-776.
339 22. Durrant JD, Votapka L, Sorensen J, & Amaro RE (2014) POVME 2.0: An
340 Enhanced Tool for Determining Pocket Shape and Volume Characteristics.
341 *J Chem Theory Comput* 10:5047-5056.
342 23. Hoffmann A, *et al.* (2012) Concerted action of the ribosome and the
343 associated chaperone trigger factor confines nascent polypeptide folding.
344 *Mol Cell* 48:63-74.
345 24. Ferbitz L, *et al.* (2004) Trigger factor in complex with the ribosome forms
346 a molecular cradle for nascent proteins. *Nature* 431:590-596.

347 25. Li X, *et al.* (2013) Electron counting and beam-induced motion correction
348 enable near-atomic-resolution single-particle cryo-EM. *Nat Methods*
349 10:584-590.
350 26. de la Rosa-Trevin JM, *et al.* (2016) Scipion: A software framework toward
351 integration, reproducibility and validation in 3D electron microscopy.
352 *Journal of structural biology* 195:93-99.
353 27. Punjani A, Rubinstein JL, Fleet DJ, & Brubaker MA (2017) cryoSPARC:
354 algorithms for rapid unsupervised cryo-EM structure determination. *Nat*
355 *Methods* 14:290-296.
356 28. Pettersen EF, *et al.* (2004) UCSF Chimera--a visualization system for
357 exploratory research and analysis. *Journal of computational chemistry*
358 25:1605-1612.
359 29. Lindorff-Larsen K, *et al.* (2010) Improved side-chain torsion potentials for
360 the Amber ff99SB protein force field. *Proteins* 78:1950-1958.
361 30. Abraham M, *et al.* (2015) GROMACS: High performance molecular
362 simulations through multi-level parallelism from laptops to
363 supercomputers. *SoftwareX* 1:19-25.
364 31. Pal S, Abraham MJ, Kutzner C, Hess B, & Lindahl E (2014) *Solving software*
365 *challenges for exascale* (Springer, Cham, Switzerland).
366 32. Bhardwaj G, *et al.* (2016) Accurate de novo design of hyperstable
367 constrained peptides. *Nature* 538:329-335.
368 33. Goddard TD, *et al.* (2018) UCSF ChimeraX: Meeting modern challenges in
369 visualization and analysis. *Protein Sci* 27:14-25.
370 34. Zhang J, *et al.* (2015) Mechanisms of ribosome stalling by SecM at multiple
371 elongation steps. *eLife* 4.

372

373

374 **Figure legends**

375 *Figure 1*. (a) Front view of the 50S subunit of the *E. coli* ribosome adapted from
376 PDB 3JBU (34), with tunnel proteins uL4, uL22, and uL29 indicated in gray. The
377 globular domain of uL23 is indicated in orange with the β-hairpin loop depicted
378 in yellow. uL24 is shown in dark blue, with the loop at the tunnel exit shown in
379 light blue. The exit tunnel, outlined by a stalled SecM nascent chain (purple), is
380 ~100 Å in length. (b) The arrest-peptide assay (8). The domain to be studied is
381 placed *L* residues upstream of the critical proline at the C-terminal end of the 17-
382 residue long arrest peptide (AP) from the *E. coli* SecM protein. A 23-residue long
383 stretch of the *E. coli* LepB protein is attached downstream of the AP, allowing us
384 to separate the arrested (A) and full-length (FL) products by SDS-PAGE after
385 translation. Constructs are translated in the PURE *in vitro* translation system
386 supplemented with wildtype, uL23Δloop, or uL24 Δloop high-salt washed
387 ribosomes for 20 min. The relative amounts of arrested and full-length protein
388 were estimated by quantification of SDS-PAGE gels, and the fraction of full-length
389 protein was calculated as $f_{FL} = I_{FL}/(I_A + I_{FL})$ where I_A and I_{FL} are the intensities of
390 the bands corresponding to the A and FL products. (c) f_{FL} is a proxy for the force
391 F that cotranslational folding of a protein domain exerts on the AP. At short
392 linker lengths, both F and $f_{FL} \approx 0$ because the domain is unable to fold due to lack
393 of space in the exit tunnel. At intermediate linker lengths, F and $f_{FL} > 0$ because
394 the domain pulls on the nascent chain as it folds. At longer linker lengths, F and
395 $f_{FL} \approx 0$ because the domain is already folded when the ribosome reaches the end
396 of the AP.

397 *Figure 2*. Structural consequences of removing the hairpin loops in uL24 and
398 uL23 modeled after PDB 3JBU of the SecM stalled ribosome. (a) In wildtype
399 ribosomes, the loop in uL24 partially obstructs the exit tunnel (top panel). Its
400 removal in uL24 Δloop ribosomes creates a wide opening into the tunnel
401 (bottom panel). (b) In wildtype ribosomes, the loop in uL23 extends into the exit
402 tunnel (top panel). Its removal in uL23 Δloop ribosomes creates an open space
403 around the area where the ADR1a domain is known to fold (8). The ADR1a
404 structure is from PDB 5A7U. (c) Cryo-EM structure of the uL23 Δloop 70 S
405 ribosome (EMD-4319), with close-up of the tunnel exit region. The PDB 3JBU
406 structure (including a 26-residue long arrested SecM AP) was fit to the cryo-EM
407 density and is displayed in ribbon representation. uL23 is in orange-red, uL24 in
408 blue, and the N-terminal end of the SecM AP that is lodged in the exit tunnel in
409 purple. There is no density for the deleted uL23 β-hairpin loop, seen in the
410 center of the image. (d) Extracted cryo-EM density for uL23 in the uL23 Δloop
411 ribosome. Wildtype uL23 (orange) and a *de novo*-built model for the mutant
412 uL23 Δloop protein (red) (PDB 6FU8) are shown in ribbon representation.

413 *Figure 3*. (a) f_{FL} profiles obtained by translation in the PURE system
414 supplemented with uL23 Δloop ribosomes (red), and uL24 Δloop ribosomes
415 (blue) in the presence of 50 μM Zn^{2+} (solid curves) or in the presence of 50 μM of
416 the Zn^2 chelator TPEN (dashed curves). (b) Δf_{FL} profiles ($\Delta f_{FL} = f_{FL}(Zn^{2+}) -$
417 f_{FL}(TPEN)) for ADR1a constructs translated in the PURE system supplemented
418 with *E. coli* ribosomes provided with the PURE kit (gray dashed), in-house
419 purified wildtype *E. coli* ribosomes (gray), uL23 Δloop ribosomes (red), and uL24
420 Δloop ribosomes (blue). (c, d) f_{FL} profiles for spectrin R15 and R16 constructs

421 translated in the PURE system supplemented with in-house purified wildtype *E.*
422 *coli* ribosomes (gray), uL23 Δloop ribosomes (red), and uL24 Δloop ribosomes
423 (blue). (e) f_{FL} profiles for titin I27 constructs translated in the PURE system
424 supplemented with in-house purified wildtype *E. coli* ribosomes (gray), uL23
425 Δloop ribosomes (red), and uL24 Δloop ribosomes (blue). Error bars show SEM
426 values calculated from at least 3 independent experiments.

427

428

429

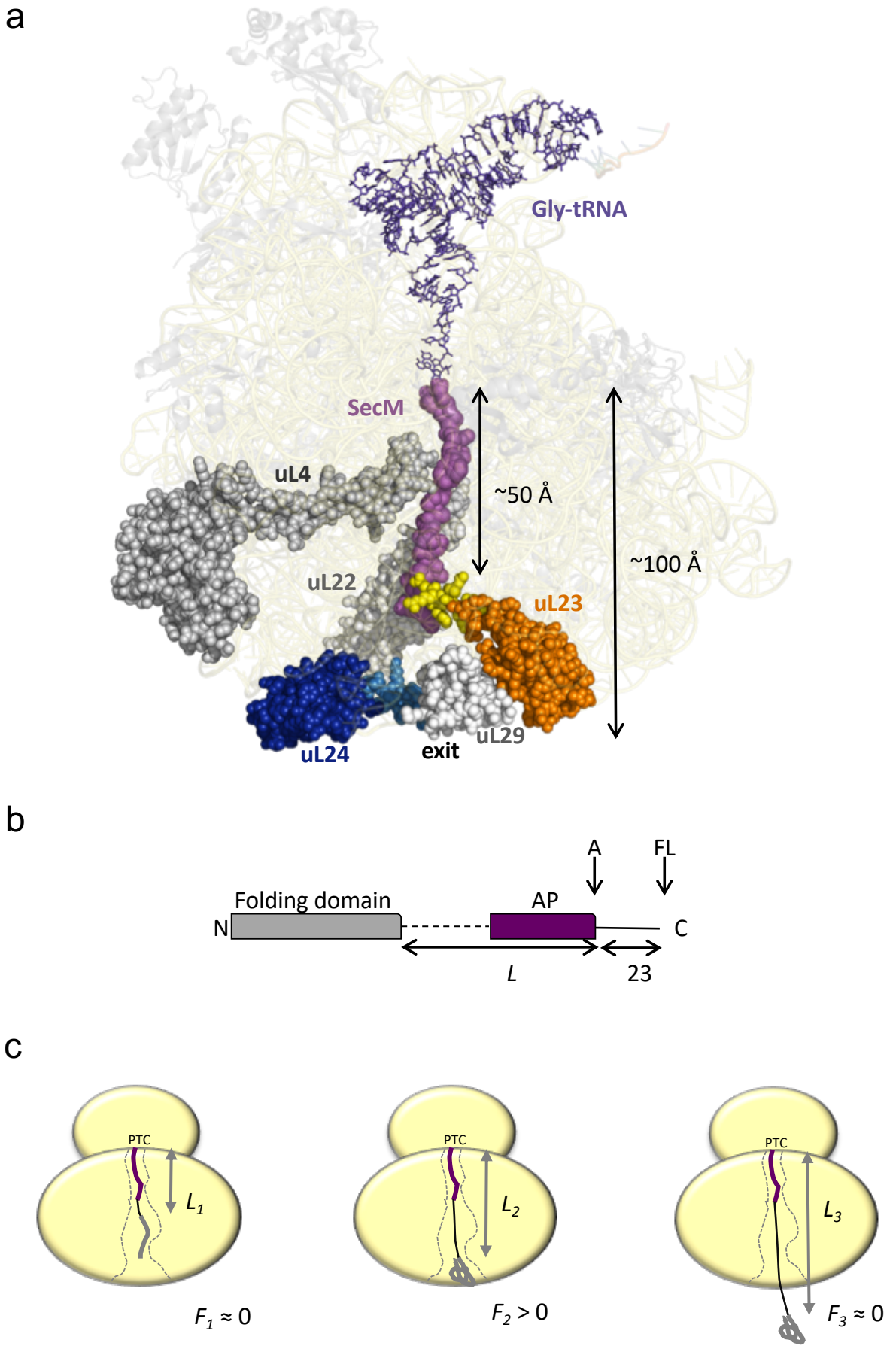
a
Gly-tRNA
SecM
uL4
~50 Å
~100 Å
uL22
uL23
uL24
exit
uL29
b
A
FL
Folding domain
AP
N
C
L
23
c
PTC
L_1
$F_1 \approx 0$
PTC
L_2
$F_2 > 0$
PTC
L_3
$F_3 \approx 0$

Figure 1

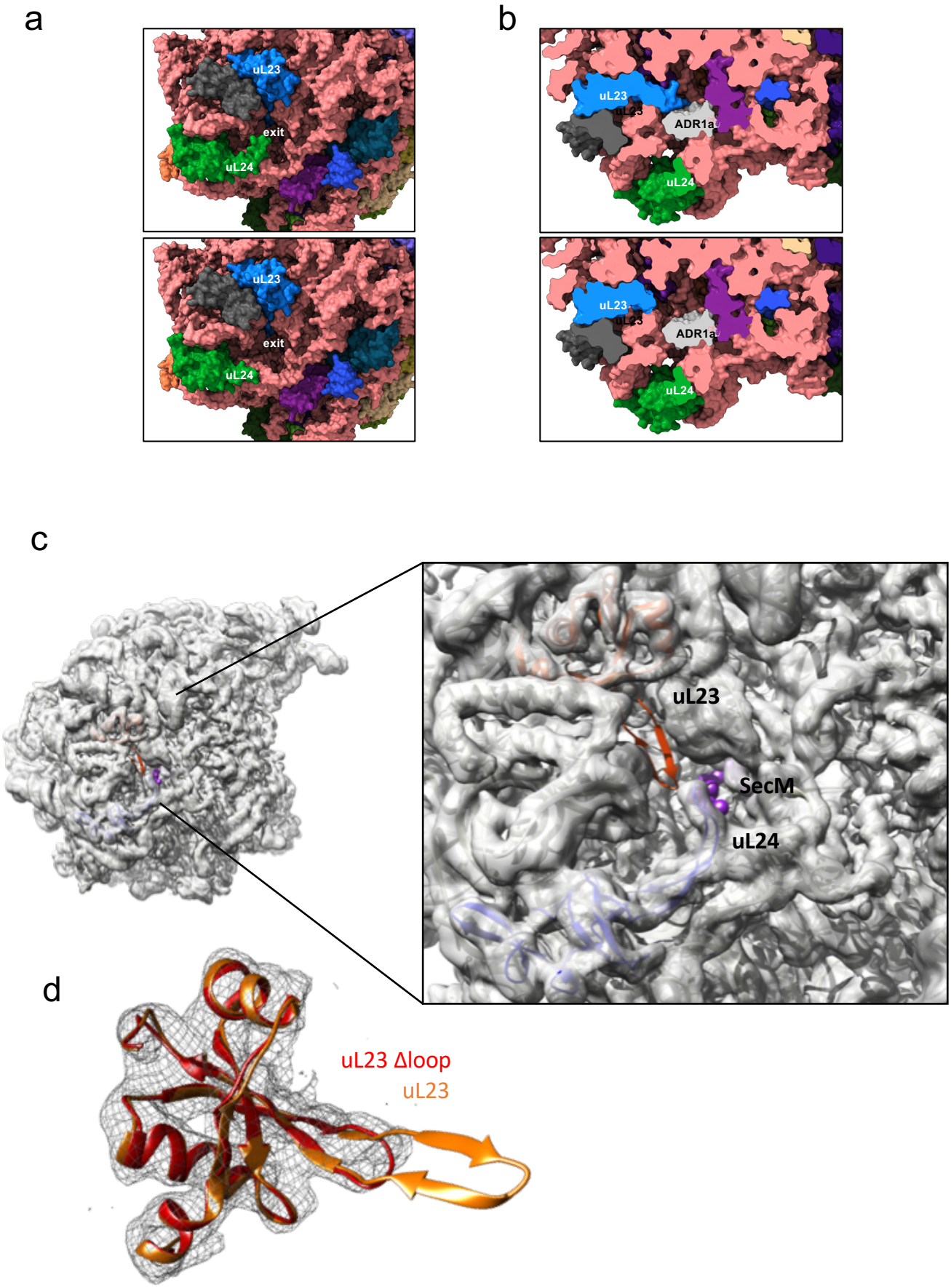
a
uL23
exit
uL24
uL23
exit
uL24
b
uL23
uL23
ADR1a
uL24
uL23
uL23
ADR1a
uL24
c
uL23
SecM
uL24
d
uL23 Δloop
uL23

Figure 2

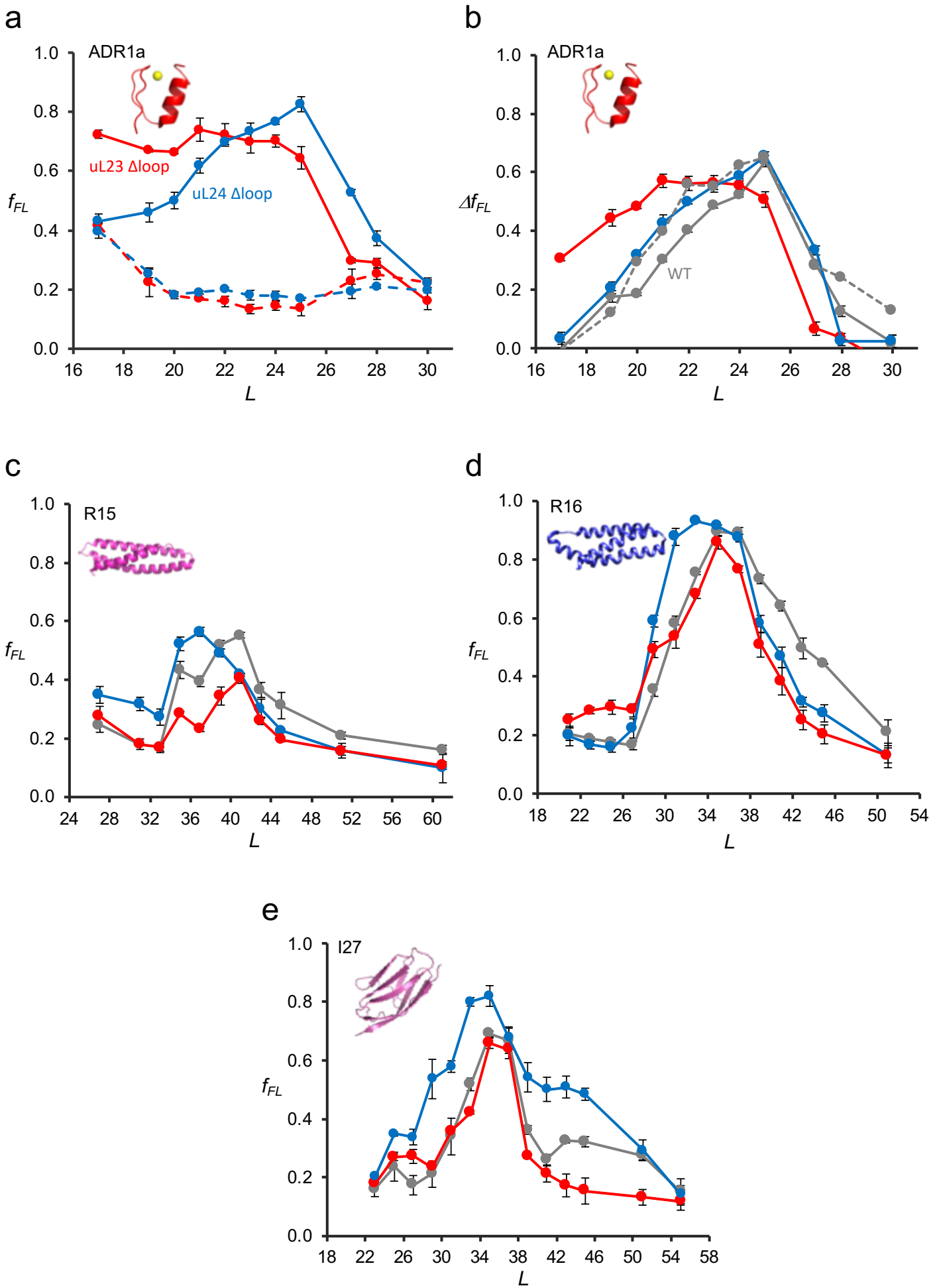
a
ADR1a
uL23 Δloop
uL24 Δloop
f_{FL}
L
b
ADR1a
WT
Δf_{FL}
L
c
R15
f_{FL}
L
d
R16
f_{FL}
L
e
I27
f_{FL}
L

Figure 3

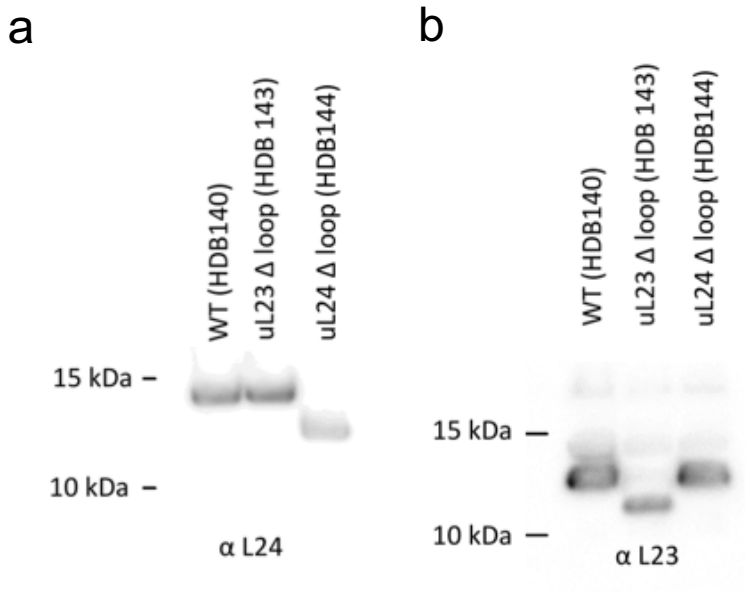

Supplementary Figure S1. A_{260} = 300 units (6.9 µM) of high-salt washed ribosomes were separated on a 12% Bis-Tris gel and transferred by Western blotting onto a nitrocellulose membrane and detected with antibodies against uL24 (panel a) or uL23 (panel b).

a

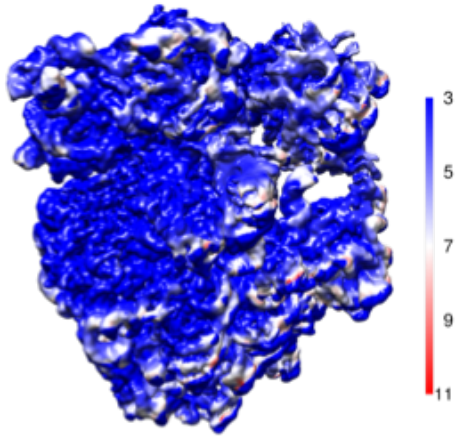

b

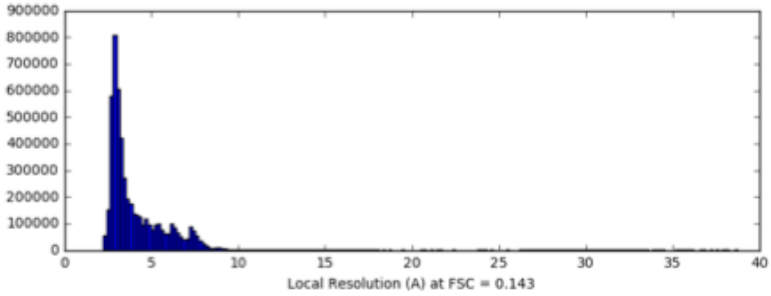

c

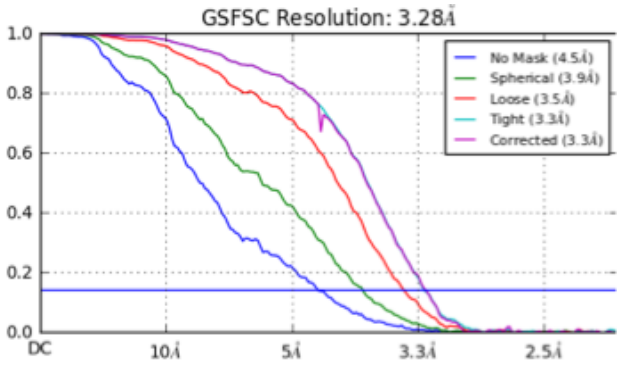

Supplementary Figure S2. Resolution map of the uL23Δ loop ribosome. (a) Calculation of the local resolution using cryoSPARC. (b) Resolution histogram at FSC 0.143. (c) Fourier-Shell correlation (FSC) curve of the refined map at 0.143 indicating an average resolution of 3.28 Å

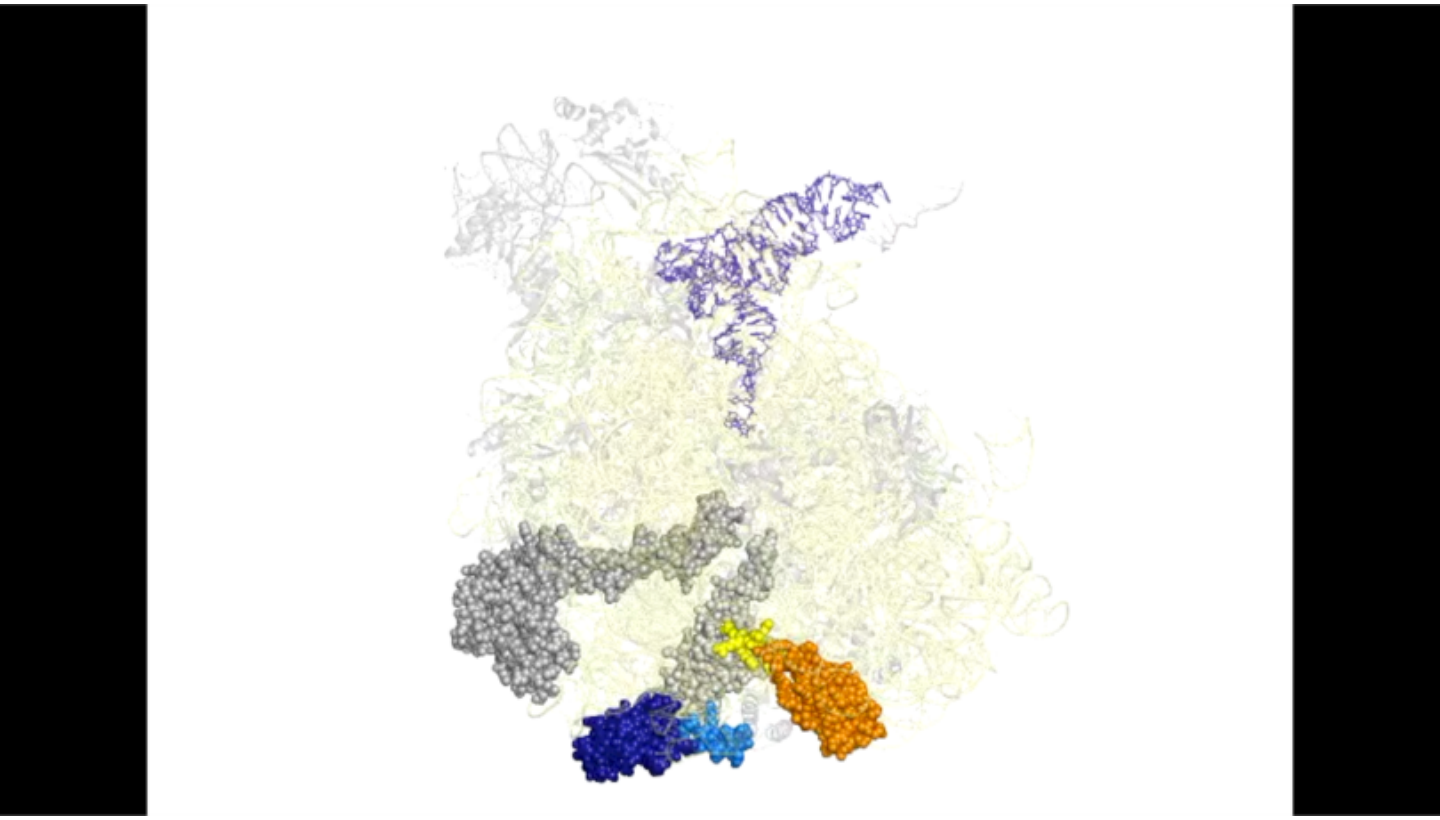

Supplementary Movie. The ribosome exit tunnel (grey mesh; calculated by the POVME algorithm) superimposed on the *E. coli* ribosome (PDB 3JBU). Coloring as in Figure 1 in the main text. The β-hairpin loops deleted in uL23 Δloop and uL24 Δloop ribosomes are shown in yellow and light blue, respectively. The volume of the exit tunnel is shown for the WT, uL23 Δloop and uL24 Δloop systems (in that order). To facilitate the visualization of the exit tunnel, spheres left out of the exit tunnel after POVME processing were manually removed.